JOURNAL OF SOLID STATE CHEMISTRY 29, 379–392 (1979)

Li_3N: A Promising Li Ionic Conductor

U. v. ALPEN

Max-Planck-Institut für Festkörperforschung, Heisenbergstrasse 1, D-7000 Stuttgart 80, Germany

Received November 3, 1978

Li_3N is presented as one of the best solid lithium electrolytes available today. Its outstanding advantages are simple preparation of crystalline as well as sintered material, stability in moist atmosphere because of a protecting surface layer, stability with elemental lithium metal up to its melting point of 813°C, high Li-ion conductivity of the order of $10^{-3}\ \Omega^{-1}\ cm^{-1}$ at ambient temperature with negligible partial electronic conductivity, and a high decomposition voltage due to a strong kinetic hindrance of the decomposition reaction. Additional work has to be focused on optimization of the Li_3N sinter preparation and on the kinetics of potential electrodes which can be used for a lithium-based battery with an Li_3N electrolyte.

1. Introduction

Lithium-based electrochemical cells provide the possibility of high cell voltages and high specific energy density because lithium is a light and highly electropositive metal. Therefore many research groups have focused their interest on lithium-based battery systems. In the past decades, the majority of research has been directed to battery systems containing a liquid electrolyte comprised of a lithium salt dissolved in an organic solvent, such as lithium perchlorate in propylene carbonate. A large number of systems with these liquid electrolytes have been proposed, some of which are in commercial production. These commercial batteries are mainly nonrechargeable, primary systems in which the negative electrode is lithium or a lithium–aluminum alloy while a variety of materials such as manganese dioxide or silver chromate have been used as the positive electrode. Some rechargeable systems in which the positive electrode is an intercalation compound such as titanium disulfide have also been demonstrated. During discharge lithium ions can be incorporated into the intercalation compounds and subsequently removed on recharging the cell. Many of these systems suffer from the fact that the organic solvents are highly reactive, toxic liquids. It is because of this that there are considerable objections concerning a large-scale application of such cells although the volumetric energy densities are outstanding, typically 5 to 10 times higher than the simple Leclanché cell. Another problem combined with that of liquid electrolytes is the sealing of the battery cells.

It can easily be seen, therefore, that solid electrolytes, which conduct lithium ions, should play an important role as materials for advanced battery systems. The all-solid-state battery of high energy density which can be produced by continuous evaporation techniques is a goal of future developments. Lithium nitride, which has recently been under extensive investigation, has been known since the last century (*1*), but did not play an active role because it seemed to be very reactive (*2*). It can be formed by the reaction of the elements even at moderate

0022-4596/79/090379-14$02.00/0

temperatures (*2, 3*) and conductivity measurements were first reported by Masdupuy (*4, 5*) 30 years ago. These pressed powders had rather poor conductivity but in the last 2 years there has been an increasing interest in studying the electrochemical properties of Li_3N in research groups, and one at Stanford University and one at the Max-Planck-Institute Stuttgart reported high conductivities in Li_3N sinters as well as in single crystals (*6–9*). These data showed Li_3N to be the best candidate for an electrolyte in a lithium-based solid state battery.

The aim of this report is to outline the electrochemical properties of Li_3N. The preparation procedure, crystal structure, and basic physical properties will only be discussed briefly as Rabenau (*10*) in a recent review has discussed the solid state chemistry and physics of this compound. The preparation and properties of Li_3N sinters will also be discussed to demonstrate the potential usefulness of this electrolyte in easy-to-fabricate future lithium-based batteries. At the end of the discussion a phenomenological model will be proposed for the understanding of the high diffusion rates of the lithium ions in Li_3N. The defect structure of Li_3N as determined by single-crystal X-ray diffraction at different temperatures (*19, 20*) is discussed as well as the results of the NMR investigations (*34*).

2. Preparation of Li_3N

The Li–Li_3N portion of the lithium–nitrogen phase diagram is a single eutectic system with the eutectic composition very close to lithium (*10, 11*) as shown in Fig. 1. Li_3N melts congruently at 813°C. The important conclusion which can be drawn from this phase diagram is the fact that Li_3N is in thermodynamic equilibrium with the solid and liquid lithium phases, respectively, over its whole range of stability. This

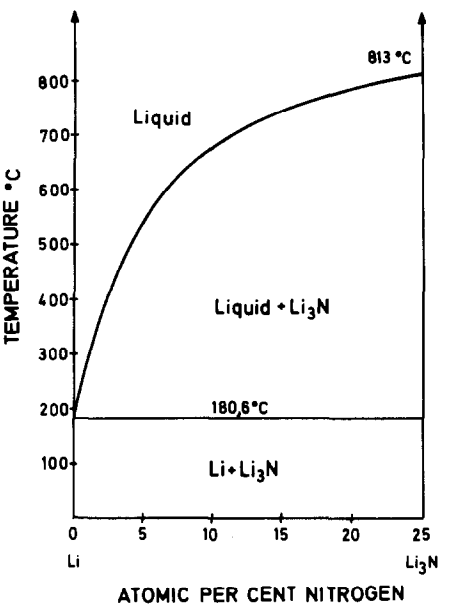

FIG. 1. The Li–Li_3N portion of the lithium nitrogen phase diagram (*10*).

outstanding feature of Li_3N makes it possible to use elemental lithium metal as the negative electrode in direct contact to the Li_3N electrolyte. The stability of binary lithium compounds such as LiI and Li_3N with the elemental lithium metal is a big advantage for the use of such materials in battery technology. Another thermodynamic factor which is of basic interest concerning the application of such a new material is the free energy of formation. This has been determined by solution calorimetry as well as by the analysis of the data of the decomposition to be ΔG_f Li_3N (198.15°K) = -129 kJ mole^{-1} (*12, 13*). This value is very small compared to those of lithium oxide Li_2O ($\Delta G_f = -560$ kJ mole^{-1}), LiOH ($\Delta G_f =$ 497 kJ mole^{-1}), and lithium carbonate Li_2CO_3 ($\Delta G_f = 1243$ kJ mole^{-1}) (*14*) which are formed on exposing Li_3N to moist atmosphere. These data explain the high reactivity of the impure Li_3N powders of early measurements.

There have been different preparation procedures for Li_3N reported in literature

(*15–17*). The interests of the solid state chemists at Stuttgart's Max-Planck-Institut for solid state research were focused on an improvement of the quality of Li_3N single- and polycrystalline material being prepared from the extremely corrosive and air-sensitive melt (*3*). The basis for an improved preparation method is very pure lithium, water, and oxygen-free nitrogen which are reacted in a scrupulously clean reaction apparatus of stainless steel. Li reacts with N_2 at a pressure of 10 atm at about 200°C and the exothermic reaction increases the temperature to 500°C. The reaction product is glassy, brown red. Li_3N single crystals can be prepared using the Czochralski technique. An important point for growing crystals of high quality is the use of tungsten crucibles, which resist attack by the melt. The crystals are pulled out of the melt during rotation at a N_2 pressure of 700 Torr which is above the equilibrium decomposition pressure. The crystals obtained are transparent and ruby red, and they can be prepared with maximum 3 cm length and 1 cm thickness (see Fig. 2).

It is quite remarkable that single crystals as well as large bars of polycrystalline Li_3N are stable in a moist atmosphere. The reason for this is that on the surface of the samples a protective thin layer of mainly LiOH with a small amount of Li_2O and Li_2CO_3 is formed and one should be aware that this surface layer may affect drastically the physical measurements. Therefore, a preparation procedure is defined which is a combination of mechanical sawing and polishing followed by a short chemical etching of the samples in a polar solvent such as methanol and subsequent drying in a glove box with a water- and oxygen-free atmosphere. Electrodes can be prepared by evaporating or sputtering Cr/Au, Mo, or W onto the sample surface which has been additionally cleaned by a glow discharge for some minutes. Lithium electrodes can be directly melted on the surfaces because Li wets lithium nitride.

3. Crystal Structure of Li_3N

The crystal structure of Li_3N has hexagonal symmetry and belongs to space group $P6/mmm$ (*15, 17*). It can be described as a sequence of Li and Li_2N layers perpendicular to the c-axis as shown in Fig. 3. The nitrogen atoms occupy the centre of the elementary cell. They are surrounded by eight lithium atoms in the shape of a hexagonal bipyramid (see Fig. 4) (*17*).

Low-temperature investigations have shown that Li_3N forms ionic bonds; its valence formula can be written as $(Li^+)_3N^{3-}$ (*18, 19*). The N^{3-} ion, which is unstable as a free ion, has been found to exist in the solid state for the first time in this compound. Lithium ions at the Li(1) and Li(2) positions (Figs. 3 and 4) form two and three Li–N bonds with lengths of 1.9 Å and 2.13 Å, respectively. The Li(2) ions are more weakly bonded to the nitrogens than the Li(1) ions. This can be seen from the thermal motion (Fig. 4). At both lithium positions the thermal vibrational amplitudes are larger perpendicular to the bond directions than parallel to them, with the largest amplitudes observed at the Li(2) positions (*17, 20*).

The defect structure (*20*) based upon the X-ray structural refinement will be presented later for a microscopic explanation of the lithium ion diffusion in Li_3N. The unusual coordination in Li_3N with the clear indication of the existence of N^{3-} ions in Li_3N will be used to explain the kinetic hindrance in the electrochemical decomposition of Li_3N.

4. Physical Investigations of Li_3N

The red color of Li_3N can be explained by optical absorption experiments at the intrinsic electronic band gap. In the orientation of $E \| c$ an indirect band gap has been found which is strongly temperature dependent between 2.05 and 2.2 eV at 300 and 4.2°K, respectively (*21*). For $E \perp c$ a shoulder in the long-wavelength region of the band gap has

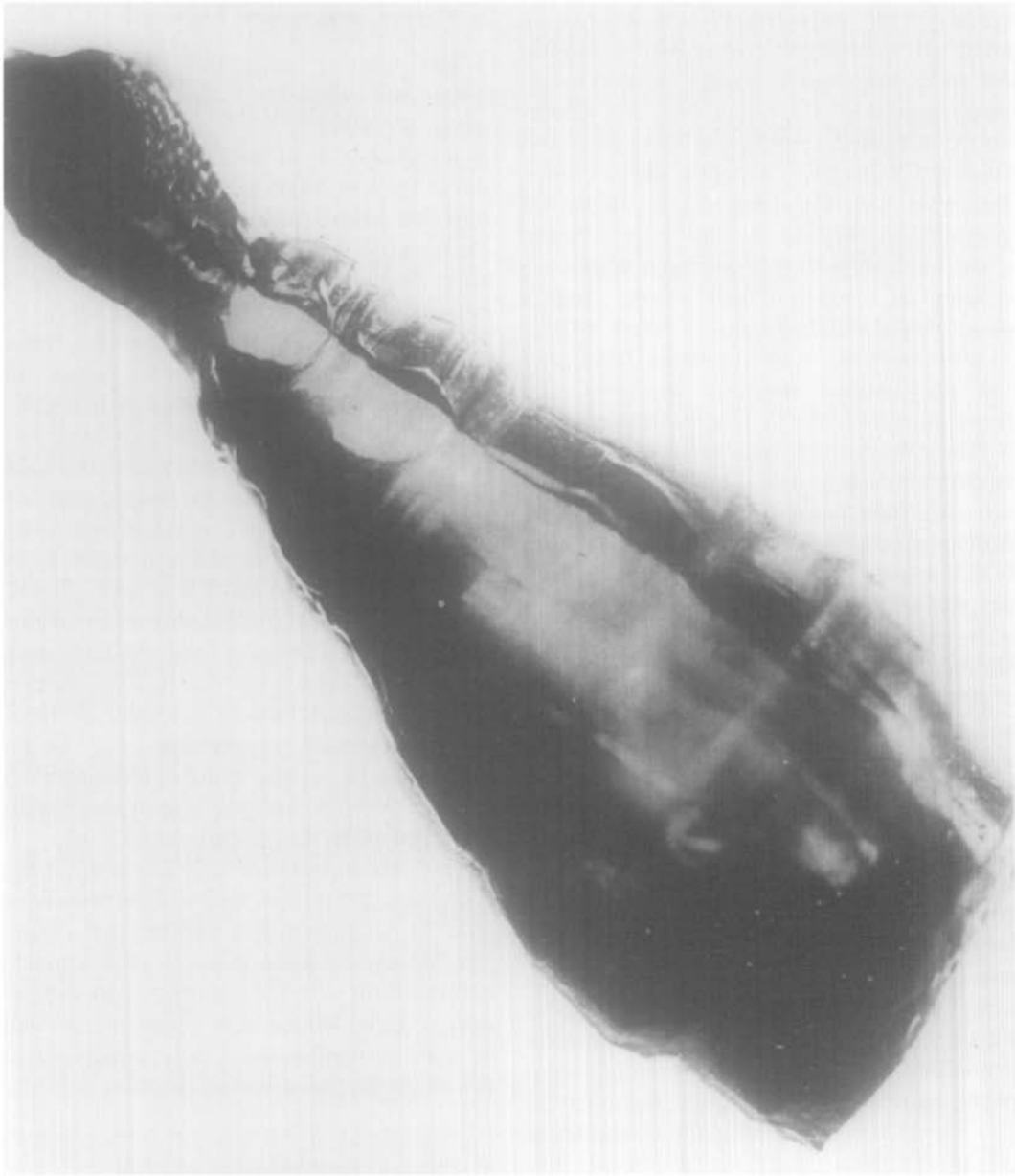

FIG. 2. Li_3N single crystal, 1 cm maximum diameter, 3 cm length; prepared by G. Müller (*3*).

been found, the height of which has been related to an annealing-induced change in concentration of intrinsic defects (*21*). The band gap of Li_3N fulfills the necessary but not sufficient condition for a good electrolyte with the requirement of low electronic transport number (*22*).

The lattice dynamics play an important role in the interpretation of the microscopic migration process in ionic conductors. The

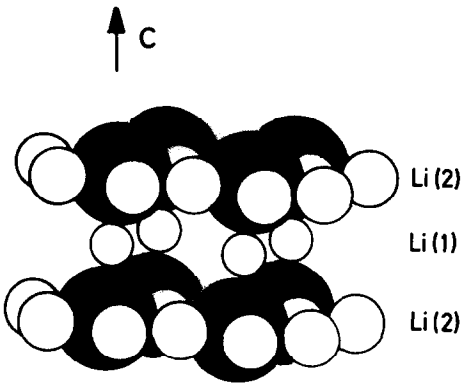

FIG. 3. Schematic representation of Li_3N structure. Solid circles show the nitrogen atoms, open circles the lithium atoms. Two Li_2N layers separated by a pure lithium layer can be seen.

highly polarizable outer electron shells of the N^{3-} ions give rise to strong dynamic screening of the Coulomb potentials which stimulates the hopping process. Li_3N is characterized by a large and anisotropic dielectric constant at room temperature of $(\varepsilon_o)_{\|c} = 6$ and $(\varepsilon_o)_{\perp c} = 10.5$ (*23, 24*). A lattice dynamic model has been set up which contains nearest-neighbor interactions and includes an anisotropic polarizability of the nitrogen ion. The phonon dispersion curves have been calculated (*23, 24*) and infrared as well as

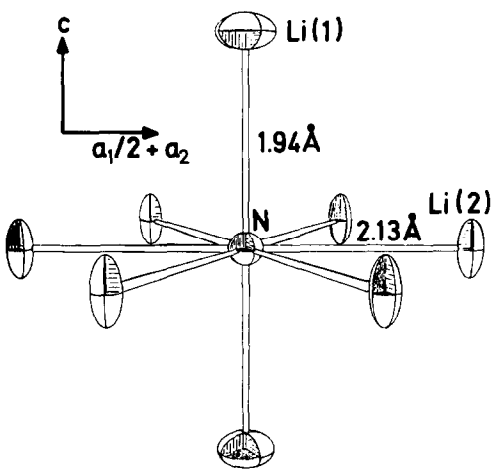

FIG. 4. Li_8N unit with the thermal vibrational ellipsoids (*17*).

Raman data well confirm these dispersion curves at the zone center. By inelastic neutron scattering data the low-lying acoustic branches of the phonon dispersion curves could be determined (*25*). It should be pointed out that the dynamic charge of the nitrogen ion in the anomalous N^{3-} state as obtained from these optical data is consistent with the X-ray scattering data. The large and anisotropic polarizability of the nitrogen which is related to a highly deformable filled $2p^6$ shell might support the high mobility of the lithium ions in Li_3N.

5. Electrochemical Investigation of Li_3N Single Crystals

A simple method for a preliminary check of the Li-ion conductivity in Li_3N is the classical transference method which is practicable with elemental Li electrodes which are stable with Li_3N. A constant current is applied to an electrochemical cell of the form

$$+Li/Li_3N/Mo-,$$

and Li-whisker formation is observed at the Mo-net cathode. The strict adherence to Faraday's law considering a lithium transference number of one cannot be proved because of the inaccuracy of the technique. But the formation of lithium whiskers in a small dc field is an indication of lithium-ion conduction in Li_3N.

The amount of partial ionic and electronic conductivities has been checked by ac as well as dc techniques.

The total conductivity has been determined by applying the complex plane impedance technique with both blocking Cr/Au and reversible lithium electrodes in both orientations of the electric field vector E parallel and perpendicular to the c-axis.

For the direct measurement of the electrochemical impedance we used a system proposed by Armstrong *et al.* using a frequency response analyzer (*26*). The frequency response analyzer is part of a data

acquisition system for electrochemical applications which has been built up on the basis of the new microprocessor computer generation with IEC-Bus interface connections (*27*). This system allows data on the temperature dependence of the electrochemical impedance to be acquired with online printing and plotting. We measured in the frequency range $10^{-2}\,\text{Hz} \leqslant \omega \leqslant 10^{+6}\,\text{Hz}$ with amplitudes of about 3 mV rms and temperatures in the range from 10 to 300°C.

The general form of the complex plane impedance diagram of a perfect single crystal with ionically blocking electrodes is a semicircle due to the electrolyte resistance, R_E, in parallel with the geometrical capacitance, C_g. This semicircle is followed by a steep increase in the imaginary part of the impedance with decreasing frequency due to the series double-layer capacitance, C_{dl}. The equivalent circuit for this idealized case is shown in Fig. 5 with the resulting complex impedance diagram. The high-frequency semicircle starts from zero on the real axis. Taking into account the low-frequency dielectric constant of Li_3N (see above), the time constant, $\tau = (R_E \cdot C_g)$, is small, about 10^{-9} sec. Therefore, the maximum frequency (1mHz) of the impedance measurement system is not high enough to determine the high-frequency semicircle. The impedance of a perfect Li_3N single crystal between blocking electrodes should only reveal the steep increase of the imaginary part of the impedance due to the double-layer capacitance. The high-frequency intercept of the impedance with the real axis gives the electrolyte resistance. In Fig. 6a an impedance diagram of Li_3N with blocking Cr/Au electrodes at a temperature of 200°C is shown. The steep increase in the imaginary part of the impedance is clearly defined.

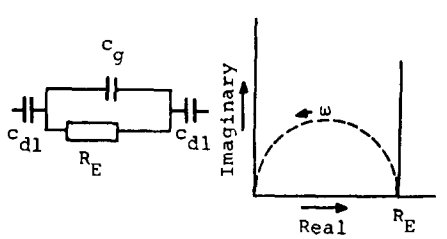

FIG. 5. Idealized equivalent circuit and resulting impedance spectrum for the blocking electrode case.

At lower temperatures, however, the impedance diagram shown in Fig. 6b is obtained. This clearly shows a semicircle which intersects the real axis at high frequency at a resistance which gives the bulk conductivity. This additional semicircle could be shown to arise from a high concentration of grain boundaries which are incorporated into the brittle Li_3N during either the growth process or the preparation procedure (*28*). This situation is similar to that of sintered polycrystalline material in which case the impedance contains an additional parallel network of a resistance and a capacitance in series with the bulk ionic resistance due to an intergranular impedance (*29*). In Fig. 7 the temperature dependence of the total bulk conductivity as obtained from the high-frequency intercept of the complex impedance diagram is shown in the well-known form of the Arrhenius plot ($\log \sigma \cdot T$ versus $1/T$).

The activation energies for lithium-ion conduction calculated from Arrhenius plots for the perpendicular and parallel *c*-axis directions show values of 0.25 and 0.70 eV, respectively (*8, 28*). The double-layer capacitance as measured with these blocking electrodes was found to be approximately temperature independent and to be about 1 $\mu\text{F cm}^{-1}$, a value which is common for ionic conductors (*30*).

With reversible lithium electrodes, however, the impedance diagrams (Fig. 8) are rather complicated (*28*). This can be explained if one considers that in this case the impedance should contain terms for charge transfer, electrocrystallization, and/or other effects, the time constants for which may overlap. This could result in the complicated shape observed. However, one can still

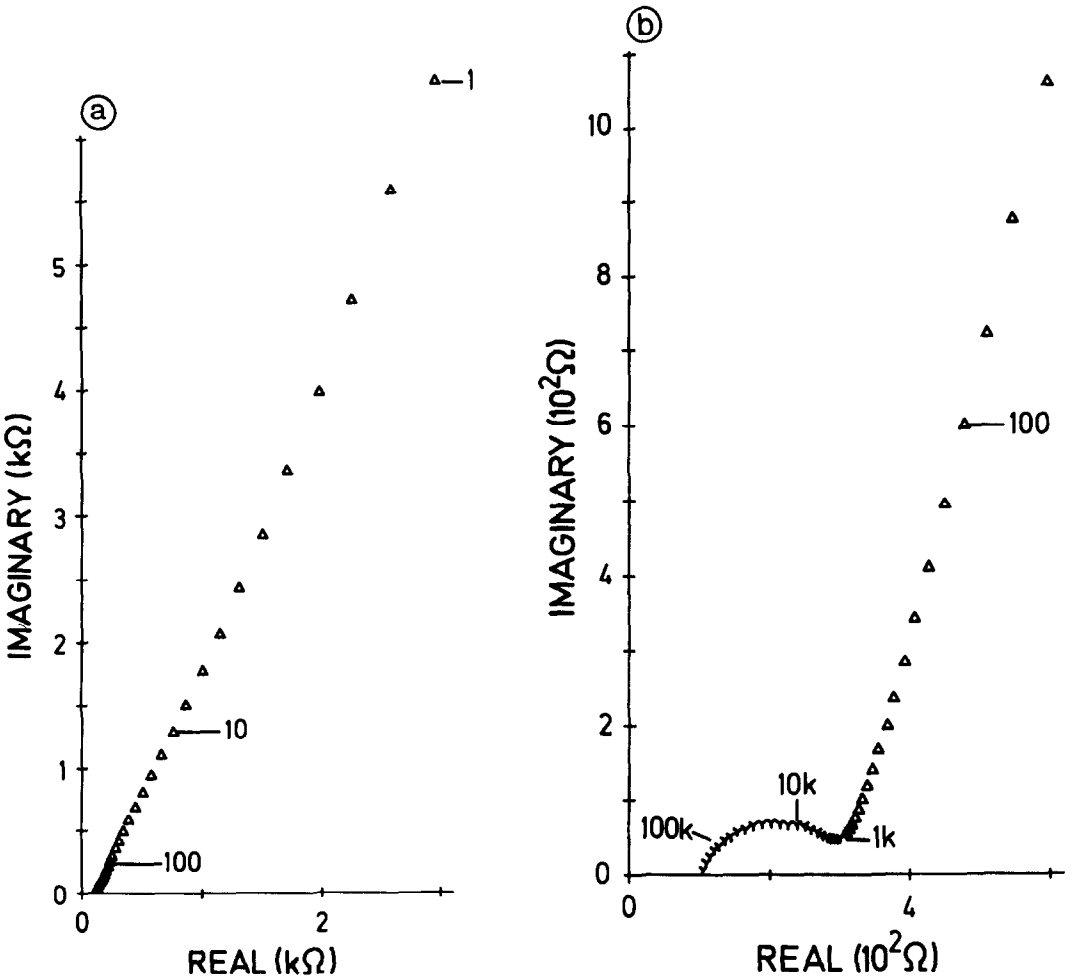

FIG. 6. Impedance diagrams for a lithium nitride crystal between blocking gold–chromium electrodes. (a) $T = 200°C$; (b) $T = 140°C$. Electrode area, 0.38 cm^2; sample length, 0.12 cm; current measuring resistance, $R_m = 10^3$ Ω. Frequencies in Hz are indicated in the plot.

obtain the electrolyte resistance from the high-frequency intercept with the real axis. The temperature dependence of the conductivity calculated from this resistance is shown in Fig. 7 and these data are consistent with previous work. Compared to the blocking electrode case, however, the conductivities with the reversible lithium electrodes are about 1 decade higher (Fig. 7), the activation energies remaining about the same. One may interpret this as an activity effect connected with the fact that in the blocking electrode case the activity is undefined whereas it is unity with reversible electrodes. Another possible explanation is that molten lithium wets Li_3N and therefore gives rise to better contact with the electrolyte.

The conductivity data reported so far clearly indicate the lithium ions predominantly diffusing in the direction perpendicular to the c-axis. The defect structure of Li_3N supports a possible model for the microscopic diffusion process

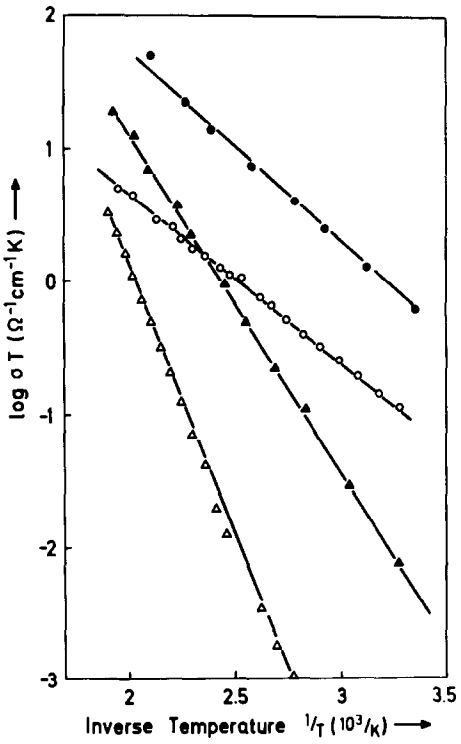

FIG. 7. Plot of the total conductivity times the absolute temperature versus the inverse of the absolute temperature. (Arrhenius plots) for the Li_3N single crystal: lithium electrodes, (●)$E \perp c$, (▲)$E \| c$; Au–Cr electrodes, (○) $E \perp c$, (△)$E \| c$.

occurring in the Li_2N plane by the Li(2) ions. It is quite unusual that the conductivity $E \perp c$ of Li_3N obeys a single Arrhenius law over a conductivity range of about 10 decades with one activation enthalpy of about 0.25 eV, a fact which has been checked by impedance, dielectric loss, and thermally stimulated current measurements from liquid helium temperatures (*31*) to 200°C (*28*).

dc experiments have been performed with blocking Cr/Au electrodes to check partial electronic conductivity and decomposition voltage. The partial electronic conductivity of single-crystalline Li_3N with two blocking electrodes was found to be extremely small, lower than $10^{-9}\ \Omega^{-1}\ cm^{-1}$ in the temperature range from 20 to 200°C with small applied bias. Attempts to measure the decomposition voltage in the above-mentioned arrangement showed that this must be much higher than that calculated from the thermodynamic data of the free energy of formation of Li_3N of 0.44 eV. No evidence of decomposition could be found over the entire potential range of some volts, suggesting that there is a substantial kinetic barrier of formation of nitrogen gas from two N^{3-}

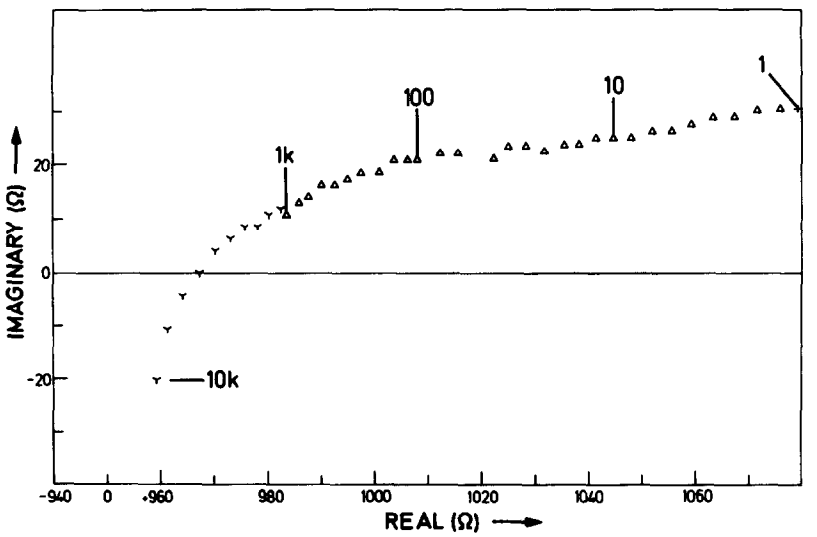

FIG. 8. Impedance diagram with lithium electrodes. Sample length = 0.12 cm; electrode area = 0.9 cm^2; temperature = 27°C; $R_m = 100\ \Omega$. Frequencies in Hz are indicated in the plot.

anions in the lattice. Therefore, this high decomposition voltage may be related to the high bond energy of N≡N of 945 kJ mole^{-1} and the existence of N^{3-} ions in Li_3N.

Current–voltage curves of Li_3N with one reversible Li and one blocking Cr/Au electrode, following the Hebb–Wagner polarization technique, have not yet successfully been performed. Further experiments are in progress to obtain the partial electronic conductivity as a function of the Li activity. Li transference in Li_3N single crystals suffers from the fact that breakdown occurs due to Li-dendrite formation in the single crystals as shown in Fig. 9. This dendrite formation is stimulated by the high concentration of grain boundaries in the single crystals giving rise to an enhanced diffusion of Li ions and atoms in the grain boundaries. After transference of some coulombs a short circuit occurs in the single crystals. Therefore, single crystals of Li_3N are well suited for the study of the anisotropy as well as that of the influence of grain boundaries on the ionic conductivity but any application of Li_3N in batteries has to be focused on the preparation of sinter material with an appropriate grain size to avoid breakdown phenomena. A commercial advantage of sinter materials is their easy and cheap preparation compared to the highly sophisticated Czochralski technique for single-crystal preparation.

6. Li_3N Sinter

Ionic conductivity of Li_3N sinters was first reported by Boukamp *et al.* (*6, 7*), revealing ambient temperature values of about $6\times10^{-4}\,\Omega^{-1}\,cm^{-1}$ for well-sintered polycrystalline material.

High-purity polycrystalline Li_3N has been synthesized in bars using the technique described in Sect. 2. These bars were milled under water- and oxygen-free atmosphere. The coarse grain size obtained lay between 10 and 200 μm. The grain size distribution had a Gaussian shape because no grain size selection was performed. Polycrystalline sinters of Li_3N were obtained by pseudoisostatic hot pressing at temperatures between 500 and 700°C and pressures between 0.5 and 3 kbar. The material obtained had densities of about 99% of the theoretical value. Figure 10 shows a scanning micrograph of a Li_3N polycrystalline pellet. The grain and grain boundaries are well defined. X-ray patterns with monochromatic MoKα radiation of the pellets indicated only the presence of pure Li_3N. ac and dc conductivity measurements were performed up to temperatures of 200°C. The conductivity was derived from the complex impedance measurements in the same way as described in section 5 on single crystals.

Generally, the impedance diagram of a sinter is rather complicated because the real bulk impedance is affected due to orientational disorder, interparticle impedance, and grain boundary conduction in addition to the electrode roughness (*32*). The impedance diagrams of Li_3N sinters may be interpreted in terms of a bulk resistance in series with a low-frequency semicircle due to the interparticle impedance (*7*). The temperature dependence of the bulk conductivity of the Li_3N sinter and the inverse intergranular resistance corrected for the sample geometry are presented in Fig. 11. With reversible lithium electrodes the conductivities observed are about two times higher compared to the conductivities obtained with blocking electrodes. We again interpret this as a contact effect, because molten Li wets the Li_3N surface, combined with an activity effect, because the lithium activity is defined with lithium electrodes. The partial electronic conductivity has been measured with blocking chromium electrodes to be about $\sigma_e \ll 10^{-10}\,\Omega^{-1}\,cm^{-1}$ at ambient temperatures. It should be pointed out that the ionic conductivity of Li_3N sinter material at ambient temperature of $1\text{–}2\times10^{-3}\,\Omega^{-1}\,cm^{-1}$ is outstanding and

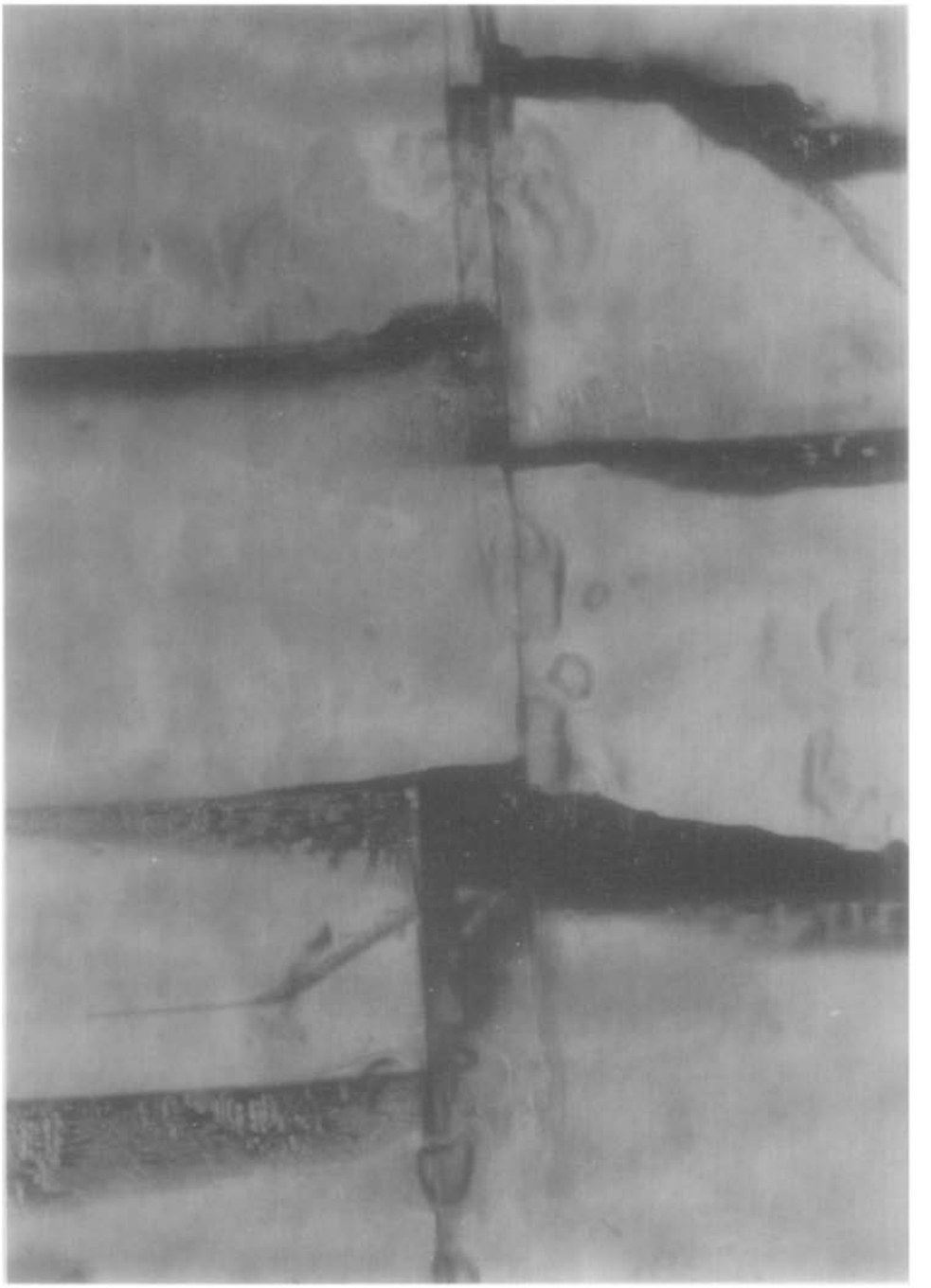

FIG. 9. Breakdown effect in a thin hexagonal plate of a Li_3N single crystal after transference of about 50 mCb Li $E \perp c$. The Li-dendrite formation takes place predominantly in the grain boundaries, giving rise to a short circuit. Magnification of the photograph, ×40 (optical transmission photograph).

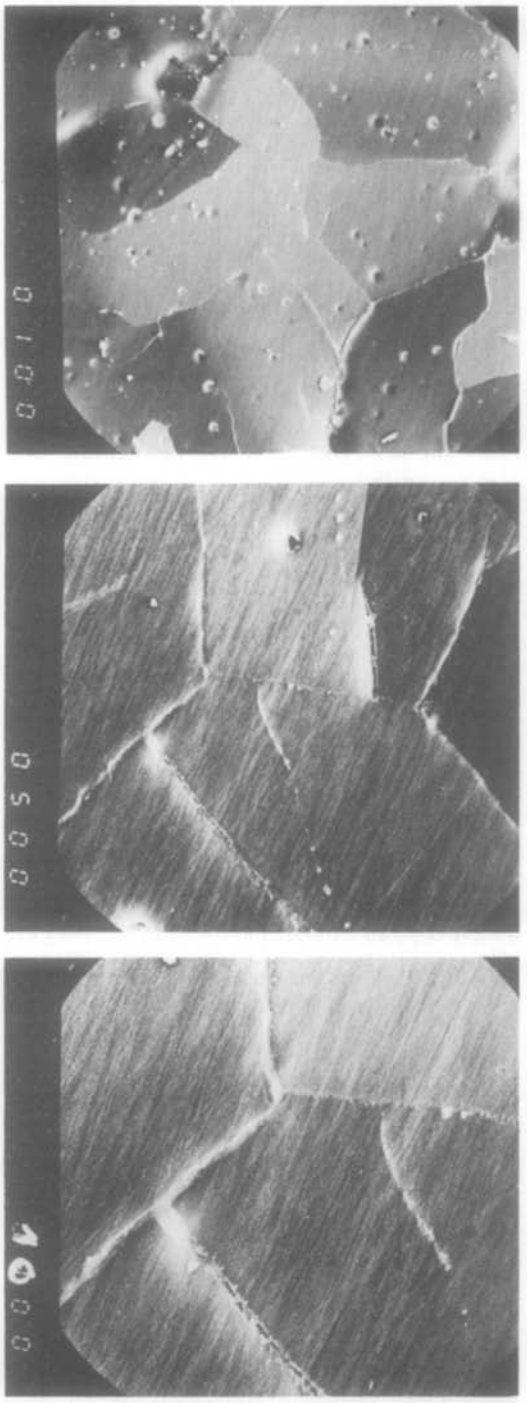

FIG 10. Scanning electron micrograph of a Li_3N sinter material with 100, 500, and 1000 magnification. The grain boundaries are well defined; taken by H. Willerscheid.

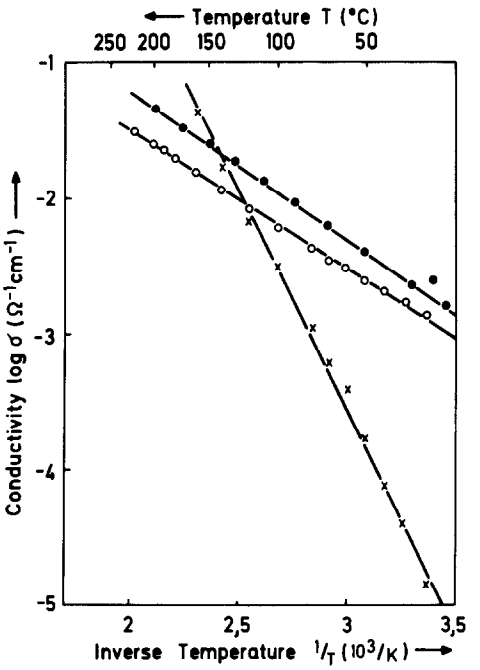

FIG. 11. Plot of the log conductivity versus inverse absolute temperature of a Li_3N sinter. (●) Bulk conductivity with Li electrodes; (○) bulk conductivity with Cr–Au electrodes; (X) inverse intergranular resistance corrected with the sample geometry.

comparable only to the conductivity data reported on Li–Na–β-alumina (*33*). No solid compound is known so far which combines the advantages of high lithium ionic conductivity and stability with elemental lithium. In addition, the low partial electronic conductivity of Li_3N sinter and the high decomposition voltage make this material a promising electrolyte for further application in batteries.

7. The Conduction Mechanism

The microscopic model for the ionic conductivity mechanism is based on the defect structure (*20*) investigated by the X-ray single-crystal diffraction studies and the NMR studies (*34*) which give information on the lithium diffusion mechanism. The defect structure proposed by Schulz *et al.* (*20*)

shows lithium nitride crystals having a natural vacancy concentration of about 1–2% at the Li(2) positions within the Li_2N layers which increases with temperature to a vacancy concentration of 3–4% at 400°C (*20*). The Li(1) sites are completely occupied. The missing Li(2) ions do not occupy interstitial sites, because no evidence of interstitials in Li_3N crystals has been found. Therefore, the investigated crystals deviate from the exact stochiometric composition in the direction of a lithium deficiency. This deviation from complete order may be related to the crystal growing procedure. A possible explanation may be the incorporation of O^{2-} ions instead of N^{3-} ions during the preparation procedure. The charge deficit at nitrogen sites can then be compensated by vacancies at the Li(2) positions. It should be mentioned that the Li(2) ions are more weakly bonded to nitrogen than the Li(1) ions. The Li–N distances and the thermal vibrational amplitudes of Li(2) ions are both significantly larger than those of Li(1) (see Fig. 4).

The vacancy concentration of the Li(2) sites of about 1–2% and the anharmonic thermal vibrations of the Li(2) ions play an important role for the interpretation of the ionic conduction mechanism of Li_3N. The ionic conduction within the Li_2N layers may be related to the Li(2) ions vibrating in shallow potential wells along the Li(2)–Li(2) connection lines. This Li diffusion along the Li(2)–Li(2) lines is shown in Fig. 12, where the residual difference electron densities in the Li_2N layer for three temperatures are shown. The ionic conduction seems to be a simple vacancy conduction in which no interstitial sites are involved.

Ionic conduction parallel to the *c*-axis may also be related to the anharmonic thermal vibration of the Li(2) ions, because the Li(1) ions do not contribute to the ionic conduction (20). The conduction process may be described by jumping Li(2) ions through a Li(1) layer. This conduction mechanism needs a higher activation energy and leads to low conductivities ($E \| c$). This is consistent with the conductivity results.

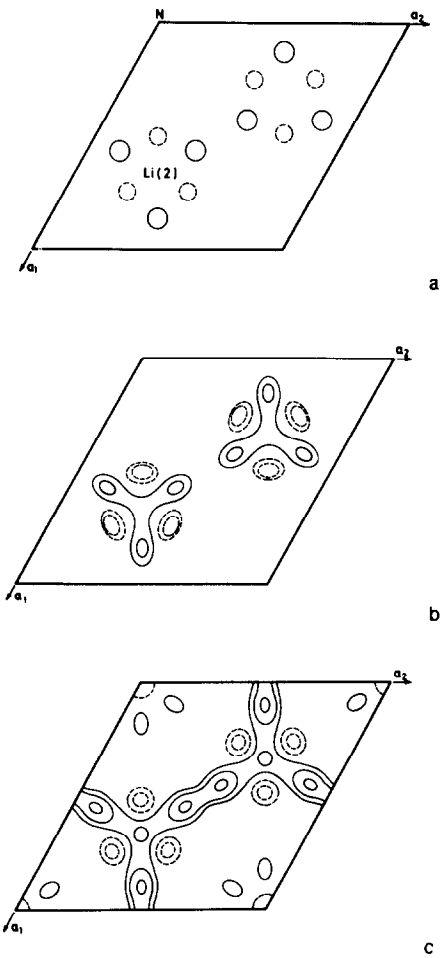

FIG. 12. Difference electron density section through the Li_2N layer at $z = 0$. Solid and broken lines represent positive and negative densities, respectively. The lines are drawn at ±0.03, ±0.06, and ±0.09 $e/Å^3$. Temperatures are (a) 120°C, (b) 315°C, and (c) 405°C (*20*).

From measurements of the quadrupole splitting and the spin-lattice relaxation time of Li^7 NMR in Li_3N Brinkmann *et al.* (*34*) present a model in which the intra- as well as inter-layer diffusion processes of Li ions together with a liquid-like behavior at high temperatures are deduced. This model differs from the above-mentioned one in that

at ambient temperature both Li systems (Li(1) and Li(2)) relax with the same time constant. Therefore, it seems conceivable that diffusion may also take place in the Li(1) layers. In both models the number of mobile ions increases with temperature. At 330°K the NMR measurements show a turning around of the relaxation anisotropy and an averaging of the quadrupole coupling constant, interpreted as an ion exchange of the Li(1) and Li(2) positions.

At 600°K the lithium diffusion attains a liquid-like behavior from the point of view of NMR. The liquid-like behavior of Li diffusion at these high temperatures may perhaps explain that the ionic conductivities parallel and perpendicular to the *c*-axis approach each other at high temperatures (*8*). Further experiments have to be done to get a consistent interpretation of lithium diffusion in Li_3N, taking into account the electrochemical as well as the structural and the NMR investigations. Therefore, it is not possible with the data available to decide whether only one Li(2) diffusion process occurs as proposed by Schulz (*20*) or two types of Li diffusion of the Li(1) and Li(2) sites are present as Brinkmann (*34*) proposed.

8. Conclusions

Li_3N may attract interest as a new electrolyte in Li-based batteries. The outstanding advantage of Li_3N compared with other Li-ion conductors is the high ionic conductivity at ambient as well as at elevated temperatures. In Table 1 the conductivity data as well as the activation enthalpy of Li motion for Li_3N single crystals and sinter are compared with some of the best-known low-temperature Li conductors available today. The stability of Li_3N with elemental lithium and the high decomposition voltage again favor this material as a separator in batteries with lithium metal anodes. It is also possible to easily fabricate Li_3N sinter material with reproducible conductivity parameters. Besides this, the reactivity of Li_3N causes difficulties in finding appropriate cathode materials which are stable in contact with Li_3N.

The scientific interest in Li_3N is mainly focused on the influence of highly polarizable ions such as the N^{3-} ion in Li_3N on various solid state phenomena as well as on the investigations of the diffusion processes leading to an enhanced Li-ion motion in Li_3N.

TABLE I

ACTIVATION ENTHALPIES *H* AND CONDUCTIVITIES OF Li_3N SINGLE-CRYSTAL AND SINTER MATERIAL COMPARED TO THE DATA OF SOME REPRESENTATIVE IONIC CONDUCTORS

Material	*H* (eV)	σ300°K (Ω^{-1} cm^{-1})	σ400°K (Ω^{-1} cm^{-1})	σ500°K (Ω^{-1} cm^{-1})	References
Li_3N s.c. $\perp c$	0.29	1.2×10^{-3}	8×10^{-3}	4×10^{-2}	(*8, 28*)
Li_3N s.c.$\parallel c$	0.49	1×10^{-5}	6×10^{-4}	8×10^{-3}	(*8, 28*)
Li_3N sinter	0.29	1.5×10^{-3}	1×10^{-2}	3×10^{-2}	(*29, 7*)
Li-β-alumina s.c.	0.19	1.3×10^{-4}	6.02×10^{-4}	5.88×10^{-3}	(*35*)
Li–Na-β-alumina sinter	–	5×10^{-3}	— Unstable —		(*33*)
Na-β-alumina s.c.	0.16	1.4×10^{-2}	5.18×10^{-2}	1.07×10^{-1}	(*35*)
Lisicon $Li_{14}Zn(GeO_4)_4$	0.56	1×10^{-6}	1.5×10^{-4}	3×10^{-3}	(*36*)
sinter	0.24	—	—	3.05×10^{-3} (524°K)	(*37*)
LiI	0.434	5.5×10^{-7}	2×10^{-5}	—	(*38*)
LiI (40 m/o Al_2O_3)	0.44	1.2×10^{-5}	1×10^{-3}	—	(*39*)

9. Acknowledgments

The excellent cooperation of Dr. M. F. Bell, Max-Planck-Institut für Festkörperforschung Stuttgart, who also revised the manuscript of this article, is gratefully acknowledged. The author is deeply indebted to Professors A. Rabenau and Heinz Schulz, Max-Planck-Institut für Festkörperforschung Stuttgart, Professor R. A. Huggins, currently at the Max-Planck-Institut Stuttgart, on sabbatical leave from Stanford University, and Professor D. Brinkmann, University of Zürich, for many fruitful and stimulating discussions.

References

1. L. OUVRARD, *C.R. Acad. Sci. Paris* **114**, 120 (1892).
2. "Gmelin's Handbuch der Anorganischen Chemie," 8 Aufl. (Gmelin, "Handbook of Inorganic Chemistry," 8th ed.).
3. E. SCHÖNHERR, G. MÜLLER, AND E. WINKLER, *J. Cryst. Growth* **43**, 469 (1978).
4. F. GALLAIS AND E. MASDUPUY, *C. R. Acad. Sci. Paris* **227**, 635 (1948).
4. E. MASDUPUY, *Ann. Chim. Paris Ser. 13*, **2**, 527 (1957).
6. B. A. BOUKAMP AND R. A. HUGGINS, *Phys. Lett. A* **58**, 231 (1976).
7. B. A. BOUKAMP AND R. A. HUGGINS, *Mater. Res. Bull.* **13**, 32 (1978).
8. U. v. ALPEN, A. RABENAU, AND G. H. TALAT, *Appl. Phys. Lett.* **30**, 621 (1977).
9. U. v. ALPEN AND G. MÜLLER, in "Electrochem. Soc., Fall Meeting, Battery Division, Atlanta, October 9–14, 1977," Abstract No. 19.
10. A. RABENAU, *in* "Festkörperprobleme" (J. Treusch, Ed.), Advances in Solid State Physics, Vol. XVIII, p. 77, Vieweg, Braunschweig (1978).
11. P. F. ADAMS, P. HUBBERTY, AND R. J. PULHAM, *J. Less Common Metals* **42**, 1 (1975).
12. P. A. O'HARE AND GERALD K. JOHNSON, *J. Chem. Thermodyn.* **7**, 13 (1975).
13. R. M. YONCO, E. VELECKIS, AND V. A. MARONI, *J. Nucl. Mater.* **57**, 317 (1975).
14. J. BARIN, O. KNACKE, AND O. KUBASCHEWSKI, *in* "Thermodynamical Properties of Inorganic Substances," Springer-Verlag, Berlin/New York (1977).
15. E. ZINTL AND G. BRAUER, *Z. Elektrochem.* **41**, 102 (1935).
16. M. D. LYUTAYA AND T. S. BARTNITSKAYA, *Inorg. Mater.* **6**, 1544 (1971).
17. A. RABENAU AND H. SCHULZ, *J. Less Common Metals* **50**, 155 (1976).
18. K. H. SCHWARZ AND H. SCHULZ, *Acta Crystallogr. Sect. A* **34**, 994 (1978).
19. H. SCHULZ AND K. H. SCHWARZ, *Acta Crystallogr. Sect. A* **34**, 999 (1978).
20. H. SCHULZ AND K. H. THIEMANN, *Acta Crystallogr. Sect. A* **35**, 309 (1979).
21. H. BRENDECKE AND E. WAGNER, *in* "Proceedings, 1977 International Conference on Defects in Insulating Crystals, Gatlinburg, Tennessee, p. 50.
22. L. HEYNE, *in* "Solid Electrolytes" (S. Geller, Ed.), Springer-Verlag/Berlin, New York (1977).
23. H. R. CHANDRASEKHAR, G. BHATTACHARYA, R. MIGONI, AND H. BILZ, *Solid State Commun.* **22**, 681 (1977).
24. H. R. CHANDRASEKHAR, G. BHATTACHARYA, R. MIGONI, AND H. BILZ, *Phys. Rev. B* **17**, 884 (1978).
25. W. PRESS, H. GRIMM, AND W. KRESS, to be published.
26. R. D. ARMSTRONG, M. F. BELL, AND A. A. METCALFE, *J. Electroanal. Chem.* **77**, 287 (1977).
27. U. v. ALPEN, K. GRAF, AND M. HAFENDÖRFER, *J. Appl. Electrochem.* **8**, 557 (1978).
28. U. v. ALPEN AND M. F. BELL, *J. Electroanal. Chem.*, in press.
29. U. v. ALPEN, M. F. BELL, AND T. GLADDEN, *Electrochimica Acta*, in press.
30. R. D. ARMSTRONG AND W. J. ARCHER, *J. Electroanal. Chem.* **87**, 221 (1978).
31. U. HOLLAND AND J. WAHL, *Bull. Amer. Phys. Soc.* **23**, 1308 (1978).
32. R. D. ARMSTRONG, T. DICKINSON, AND P. M. WILLIS, *J. Electronal. Chem.* **53**, 389 (1974).
33. G. C. FARRINGTON AND W. L. ROTH, *Electrochim. Acta* **22**, 767 (1977).
34. D. BRINKMANN, W. FREUDENREICH, AND J. ROOS, *Solid State Commun.* **28**, 233 (1978).
35. M. S. WHITTINGHAM AND R. A. HUGGINS, *in* "Solid State Chemistry" (R. S. Roth and S. J. Schneider, Eds.), p. 139, Nat. Bur. Standard Special Pub. 364 (1972).
36. U. v. ALPEN, M. F. BELL, W. WICHELHAUS, K. Y. CHEUNG, AND G. J. DUDLEY, *Electrochim. Acta* **23**, 1395 (1978).
37. H. Y.-P. HONG, *Mater. Res. Bull.* **13**, 117 (1978).
38. C. R. SCHLAIKJER AND C. C. LIANG, *J. Electrochem. Soc.* **118**, 1447 (1971).
39. C. C. LIANG; *J. Electrochem. Soc.* **120**, 1289 (1973).